Titanium Dioxide for Water Purification

Subjects: Nanoscience & Nanotechnology

Contributor: Sanja J. Armaković , Maria M. Savanović , Stevan Armaković

Titanium dioxide (TiO_2), one of the most frequently used materials in general, has emerged as an excellent photocatalytic material for environmental applications. Here, principles and mechanisms of the photocatalytic activity of TiO_2 have been analyzed. Structural and physical specificities of TiO_2 nanoparticles, such as morphology, crystal structure, and electronic and optical properties, have been considered in the context of photocatalytic applications.

TiO2 nanoparticles photocatalytic degradation processes physical properties operational parameters superhydrophilicity

1. Structural Features and Physical Properties of TiO_2 Nanoparticles

Understanding the fundamental properties of semiconductor materials governing their photoelectric performance (such as their crystal structure, lattice parameters, and optical and electronic properties) is essential to optimize their performance for photocatalytic applications. This section introduces the fundamentals underlying the photocatalytic performance of nanostructured TiO_2.

1.1. Crystal Structures of TiO_2

Morphology and the crystal structure of TiO_2 principally determine its photocatalytic activity. Therefore, essential factors for TiO_2 photocatalytic activity are crystallite size and the specific surface area [1][2][3]. TiO_2 nanostructures with different shapes and titania-based nanocomposites have attracted much attention in research due to their diverse physicochemical characteristics. The 1D TiO_2 nanostructures have gained more attention compared to their 0D and 2D counterparts due to the higher aspect ratio, increased surface area, and efficient electronic charge properties [4]. TiO_2 exists in two tetragonal forms (rutile and anatase) and one rhombic form (brookite), **Figure 1** [5][6][7][8]. Brookite is difficult to obtain in laboratory conditions, while rutile and anatase are easily prepared. As a bulk material, rutile is the stable phase; however, solution-phase preparation methods for TiO_2 generally favor the anatase structure. These observations are attributed to two main effects: surface energy and precursor chemistry. It has been found that the surface energy of anatase is lower than those of rutile and brookite [8]. The concept of surface energy accurately explains the observed crossover size of about 30 nm where anatase nanoparticles transform to rutile [9]. Secondly, the crystal structure stability has been explained based on a molecular picture. The precursor chemistry determines the nucleation and growth of the different polymorphs of TiO_2, which depends on the reactants used [10][11]. A complicating factor in understanding nanoparticle formation is the multitude of

experimental conditions used to synthesize the different TiO_2 phases, making it challenging to compare mechanisms [8][12].

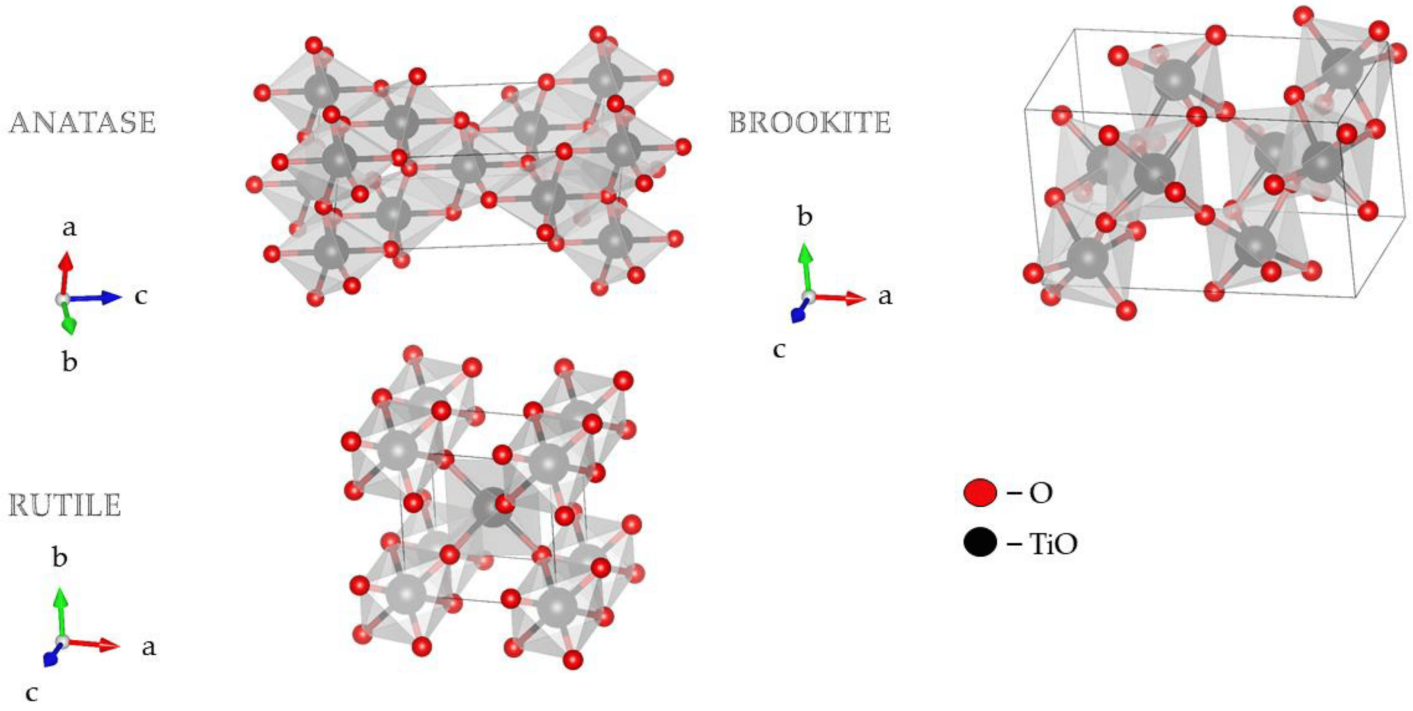

Figure 1. 3D visualization crystal structures of TiO_2 using visualization for electronic and structural analysis (VESTA) [13].

These polymorphs, anatase, and rutile, exhibit different properties and, consequently, different photocatalytic performances. Of the two tetragonal forms mentioned, the anatase form shows significantly higher photocatalytic activity than rutile due to the higher presence and nature of surface hydroxyl groups. Transformation of anatase form to rutile happens at elevated temperatures of 700–1000 °C. Anatase form is stable at lower temperatures (it occurs in the form of a pyramidal crystal structure). At the same time, rutile (needle-shaped) is dominant during the synthesis at high temperatures [14][15][16]. Anatase has a higher energy gap, which additionally contributes to the photocatalytic activity of this form. The energy gap of anatase is 3.20 eV, while the rutile energy gap is 3.02 eV [17][18].

TiO_2 Degussa P25 is the most frequently used commercial product containing 75% of anatase form and 25% of rutile form [19][20]. The mentioned mixture exhibits outstanding photocatalytic performance and superiority compared with other TiO_2 [21]. The predominant form of titania used is anatase. It was found that anatase is the most photocatalytic active form within TiO_2 polymorphs. TiO_2 Hombikat is a pure anatase form of photocatalyst [19]. TiO_2 also appears in another form named TiO_2 Wackherr “oxide de titan standard”, which contains 100% of anatase form, exhibits interesting characteristics related to photocatalytic application, and is more efficient than TiO_2 Degussa P25 [22][23][24]. The main characteristic of this photocatalyst, when compared with TiO_2 Degussa P25, is a lower scattering of radiation in the UV area, which is most likely the consequence of the greater size of particles. Particle size is a crucial factor affecting the performance of nano-photocatalytic materials. The greater size of TiO_2 Wackherr particles than TiO_2 Degussa P25 results in a lower specific surface area. Particles with a

lower specific surface area usually exhibit low photocatalytic activity. However, they can be more efficient in photocatalysis, where optical properties and low scattering are significant [24][25].

1.2. Electronic Structure of TiO_2

Understanding the electronic properties of semiconductor materials, including their band structure, nonequilibrium carrier concentration, carrier mobility, and lifetime is essential to achieve inflection of charge carrier behavior and enhancing photocatalytic performance. Against this background, electronic properties of anatase, rutile, and brookite TiO_2 phases were introduced [26]. The current understanding of the electronic structures of TiO_2 is mainly based on the results of independent and combined theoretical calculations, usually in the framework of the density functional theory (DFT) [6] and experimental techniques (e.g., synchrotron radiation photoelectron spectroscopy, UV-vis spectroscopy, ultraviolet photoelectron spectroscopy, and photoluminescence) [27][28].

The application of various computational methods in elucidating the photocatalytic properties of novel TiO_2-based materials is essential. Namely, applying the DFT approach enables researchers to predict the band gap of newly designed materials and focus their attention on synthesizing materials with target photocatalytic properties. The computational aspect of band-gap engineering is critical in developing new photocatalytic materials, as this parameter is essential for practical applications [29]. Additionally, the DFT approach, in combination with carefully selected density functionals and basis sets, is an excellent tool for understanding the light absorption properties of molecules that are degraded by photocatalysts, helping scientists to easier identify the degradation mechanism [30].

Regarding the computational design of novel materials, the DFT approach offers the best cost–efficiency ratio [31]. This flexible theoretical approach allows researchers to elucidate the structural and electronic properties of photocatalytic materials by analyzing how various structural alterations influence the electronic subsystem of nanomaterials.

However, the DFT approach's severe drawback is that it severely underestimates the band gap values due to self-interaction error [32][33][34][35]. Considering the fundamental importance of band gaps in photocatalysis, this is a significant challenge in designing novel compounds to be applied in this area. In general, this issue can be tackled in two main ways. One approach is to create specially designed density functionals that reproduce electron density adequately. The second approach is to use the existing density functionals and implement specific corrections within them. Both directions have positive and negative sides. For example, specially designed hybrid density functionals yield outstanding results in accuracy, but they are computationally much more demanding and are usually applicable only for single-point band structure calculations. Conversely, corrected density functionals offer improved results over conventional density functionals, with computational costs slightly more demanding than traditional density functionals.

Considering the application of hybrid functionals for band structure calculations, it is worth mentioning the importance of the HSE06 hybrid functional [36]. Recent studies have confirmed this function's importance in predicting band gaps of different materials with small, intermediate, and large values of this critical parameter [37]

[38]. However, in terms of computational costs, hybrid density functionals may still be unavailable to significant number of research groups, which may apply the computationally affordable DFT + U method [39]. This method adds a Hubbard-like term to the Hamiltonian to account for on-site interactions. The simplest version of the DFT + U approach relies on only one parameter—on-site Coulomb term (*U*). However, this method can be improved by incorporating the site exchange term *J*. *U* and *J* parameters can be obtained through ab initio applications. Still, they are frequently obtained empirically by testing a range of values. So far, many research studies have reported the values of these parameters for certain types of materials, so a literature survey is warmly recommended to find good starting values.

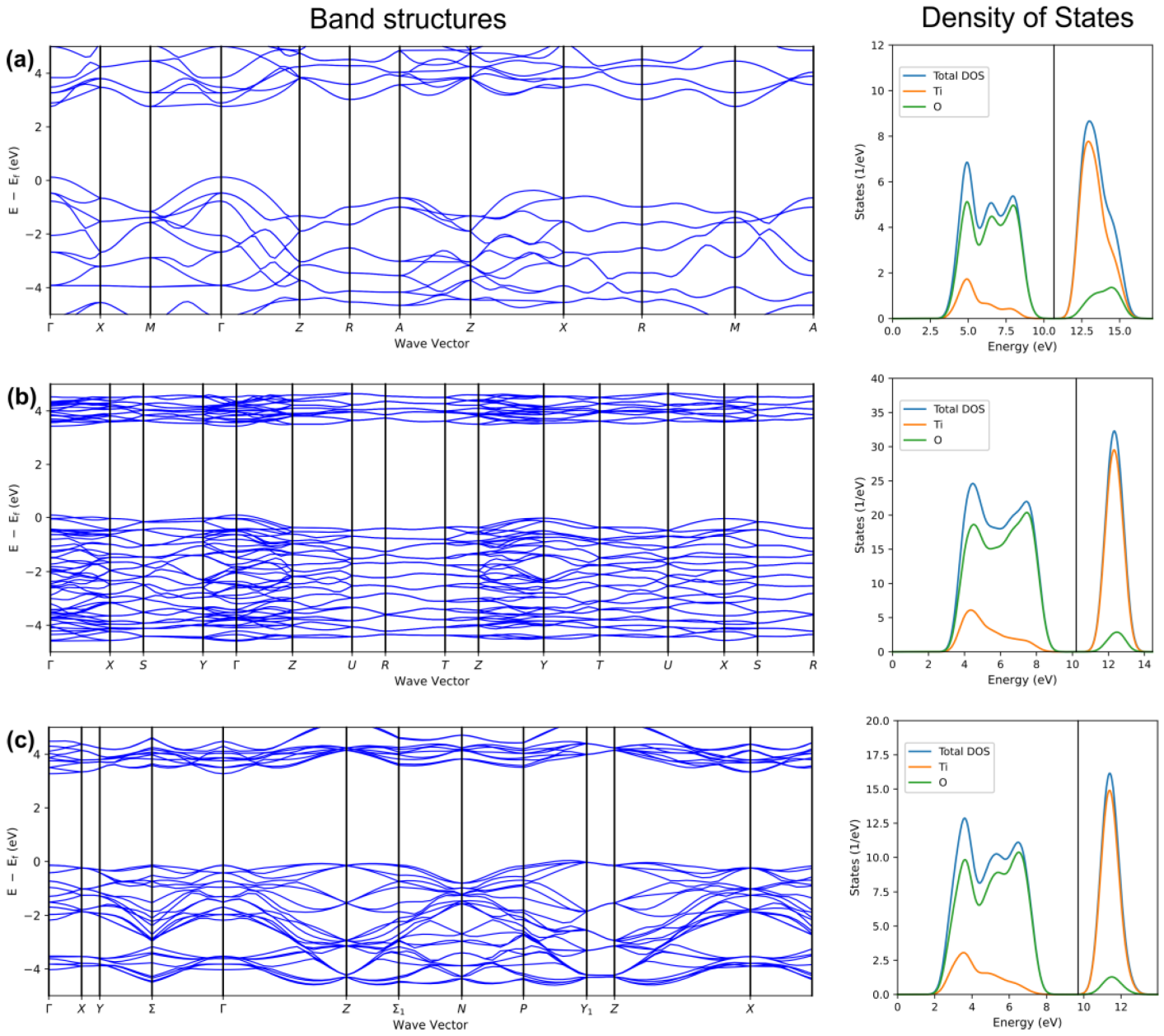

Figure 2. Band structures (left panel) and projected density of states (right panel) for the (**a**) rutile), (**b**) brookite, and (**c**) anatase polymorphs of TiO_2, as obtained by DFT+U calculations (PBE functional, GBRV pseudopotentials, ,) in Quantum Espresso program as implemented in Schrödinger Materials Science Suite 2022-4.

In **Figure 2**, the band structures and density of states as obtained by applying the DFT + U method are presented, with *U* taking the value of 7.8 eV and *J* taking the value of 1 eV, as reported in studies by [40][41]. Inspection of band structures shows that the application of the DFT + U method provides results for band gaps that are in agreement with experimental results, which will be mentioned somewhat later. The density of states figures also show that the conduction band consists of Ti states, while valence band (VB) consists of O states. As reported in reference by Li et al. [42], CB consists of Ti_{3d} states, while VB consists of O_{2p} states.

Ordinarily, TiO_2 phases, especially anatase, show good insulation in their ideal stoichiometric states due to their wide bandgap [43]. However, certain types of point defects are unavoidably introduced during the preparation process. These defects might be interstitial titanium ions (T^{3+}), oxygen point defects, and substituted ions and can notably affect the charge carrier behavior, band structure, and, eventually, photocatalytic performance [44]. The characteristics of defects (e.g., concentration, type, distribution, and dimension) and their influence on the photoinduced charge carriers in TiO_2 can be various [45]. Point defects can induce the generation of defect states, the position generally influenced by the surface and phase. For instance, the defect states of rutile-TiO_2 (110) and anatase-TiO_2 (101) are found at ≈0.8–1.0 eV and ≈0.4–1.1 eV, of which both are below the CB edge [46]. In the brookite phase, both rutile-like (Y-shaped) and anatase-like (T-shaped) OTi_3 building blocks exist, inducing the O_{2p} in VB to present characteristics from both tetragonal phases [6]. Considering the application of hybrid and recently developed density functionals, the study by Dharmale et al. is worth mentioning. In their work, electronic properties such as effective mass, the partial density of states, the total density of states, and the band structure of brookite TiO_2 have been studied by applying using seven exchange-correlation functionals, including the already-mentioned HSE06 [47]. Band structures and projected density of states for the rutile), brookite, and anatase polymorphs of TiO_2 are shown in **Figure 2**.

1.3. Optical Properties of TiO_2

A semiconductor's optical properties (e.g., photoconductivity, dielectric constant, refractive index, extinction coefficient, reflectivity, absorption coefficient, and loss function) are related to its bandgap [48]. TiO_2 is commonly known as a wide-bandgap semiconductor with high susceptibility to UV light [49][50]. The optical absorption in the visible and near-infrared regions is insignificant because photons in the visible region do not have intrinsic excitation of carriers. When the electrons (e^-) in the VB are exposed to UV radiation, they are excited to the CB, leaving holes (h^+) in the VB [51][52][53]. The CB e^- is now in a purely 3D state, and the possibility of transition of e^- to the VB is reduced due to the difference in parity. Therefore, the probability of e^-–h^+ recombination is reduced [54]. Consequently, separating energy between these two states defines the sensitivity of TiO_2 towards the light in the UV range. However, the optical properties at the surface differ considerably from those of the bulk material, providing extensive opportunities to optimize further the photoelectric and optical properties of TiO_2 [55].

The bandgap energies (i.e., optical absorption edges) of rutile, anatase, and brookite TiO_2 are estimated to be ≈3.00, 3.21, and 3.13 eV at room temperature, respectively. The photon energy values of optical absorption edges of rutile and anatase increase with the crystal growth temperature decrease [8]. Overall, rutile and anatase bandgaps in bulk are considered to be indirect [56]. Detailed examinations of rutile TiO_2 at temperature 1.6 K

discover an anisotropic optical response characterized by a direct forbidden transition at ≈3.06 eV. At the same time, the bandgap near the edge is prevailed by an indirect transition. The direct bandgap transition of anatase occurs at ≈3.8–4.0 eV [57]. Additionally, the orthorhombic TiO_2 brookite bandgap energy has been experimentally determined to be 3.1–3.4 eV. This is a biaxial material with three independent components other than the dielectric tensor of the uniaxial rutile and anatase materials [8][58]. The significant value of the energy gap limits the exceptional photocatalytic characteristics of TiO_2. Namely, the photon energy should be high enough to excite the TiO_2 particles.

In recent experimental and theoretical investigations, efforts have been made to improve the optical properties of TiO_2 by increasing its photosensitivity and identifying the correlation between its surface, interfacial, and microstructural characteristics and the corresponding mechanisms crucial to its photoelectric properties [59][60]. Generally used strategies to enhance the optical properties of TiO_2 include element doping [61][62] coupled with other semiconductors to form heterojunctions [63][64], synthesis of nanostructures with particular morphologies [65], surface sensitization to improve optical characteristics using organic dyes, metal nanostructures or metal complexes [66] and so on.

The doping technique can be explained as the deliberate addition of impurities into a semiconductor material (**Figure 3**). To enhance TiO_2 catalytic activity under visible light, metal/non-metal-doped TiO_2 structures have been extensively studied [67]. Adding metal/non-metal increases oxygen vacancies and reduces the band gap energy, resulting in higher photocatalytic activity [68]. This could be useful in wastewater treatment for the photocatalytic degradation of organic compounds under visible and UV light radiation. Many different metals, such as Pd [69], Pt [70], Au, Ag [71], Ce [72], Sr [73], V [74] and so on, have been employed for the preparation of metal-doped TiO_2 catalysts.

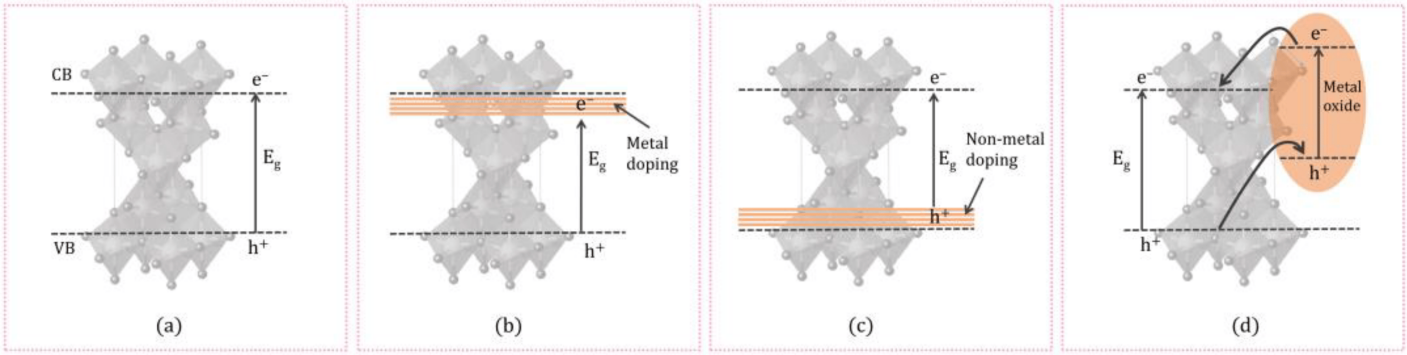

Figure 3. Illustrating the generation of photoinduced e^- and h^+ in (**a**) pure TiO_2, (**b**) metal-doped TiO_2, (**c**) non-metal-doped TiO_2, and (**d**) coupling TiO_2 with the metal oxides.

The sol–gel method is often used in the synthesis, where the photocatalyst is doped with metals such as Fe, Ni, Cr, V, La, Nd, and Sm. The sol–gel process represents one of the versatile methods for preparing nano-dimensional materials. Incorporating an active dopant allows the doped element to interact directly with the support, which is why the material has catalytic or photocatalytic properties. When metal nanoparticles are doped into the TiO_2, a

new energy level or an interband state is produced in the band gap close to the CB arising from the partially filled d orbitals of the doping metal ions modifying the electronic structure and hence lowering the band gap (**Figure 3**b).

Although metal-ion doping decreases the energy gap of TiO_2, the aforementioned metal ions can also act as recombination centers for electrons and holes, thus reducing the overall activity of the TiO_2 [75]. In recent years, non-metals such as C, N, P, S, and B have been the best candidates for obtaining the desired band-gap narrowing of TiO_2 [76]. It was shown that non-metal doped TiO_2 shows significant catalytic activity under visible light radiation [77]. Several researchers have depicted that TiO_2 doping with non-metal ions improve photocatalytic efficiency compared to metals. Doping with cations changes the morphology of the photocatalysts and the photocatalytic activity. It also affects the photocatalyst's electronic structure. Non-metal dopants influence the VB of TiO_2 through interactions with 2p e^- of O and form an impurity level above the VB. Distinct non-metals, including N, C, S, F, B and so on, are used as dopants and have shown promising outcomes in recent research studies. Nitrogen doping in TiO_2 has gained considerable attention due to its ability to narrow the band gap and promote the electron–hole pair transfer mechanism (**Figure 3**c). It has been observed that in the case of doping with lighter elements such as N, C, S, or B at substitutional sites of TiO_2, lower atomic number elements with smaller effective nuclear charge appear at a higher localized energy level in the band gap. Doping TiO_2 by carbon stabilizes anatase TiO_2, enhances its conductivity, and extends the pollutant adsorption on the surface of TiO_2 [78].

Žener et al. [68] showed that doping, co-doping, and modifying TiO_2 samples with nitrogen, sulfur, and platinum increased their photocatalytic activity by up to 6 times. XRD measurements revealed that the replacement of HCl with H_2SO_4 during sol–gel synthesis reduced the size of the crystallites from ~30 nm to ~20 nm, increasing the surface area. This is consistent with the samples' photocatalytic activity and the photocatalysts' measured photocurrent behavior [68].

Coupling TiO_2 with the metal oxides increases the charge carrier separation and thereby increases the lifetime of the charge carriers [79]. When the coupled catalyst, consisting of TiO_2 and a semiconductor, is irradiated, both the TiO_2 and the semiconductor will excite electrons from VB to the CB using UV and Visible irradiation. TiO_2 and the semiconductor configuration for coupling are crucial for the enhancement activity. The CB of TiO_2 should be more favorable than the corresponding band of the semiconductor, and the VB should be more cathodic than that of TiO_2. The e^- from the CB of the semiconductor migrates to the CB of TiO_2 and increases the concentration of electrons at the TiO_2 conduction band. At the same time, the h^+ generated at the VB of TiO_2 will be transferred to the VB of the semiconductor, increasing the concentration of h^+ in the coupled semiconductor/TiO_2 (**Figure 3**d) [80] [81][82]. Couplings of TiO_2 with a metal oxide such as ZnO [83], SiO_2 [84], Cu_2O [85], Bi_2O_3 or $ZnMn_2O_4$ [86], graphene [87] and so on. are reported for many photocatalytic applications including organic pollutant degradation, water splitting, pharmaceutical degradation and so on. TiO_2–ZnO binary oxide systems containing various molar ratios of TiO_2–ZnO were prepared using a sol–gel method. It was reported that the crystalline structure, thermal stability, and porous structure parameters were determined by the molar ratio of TiO_2 to ZnO and the calcination process for the most part. TiO_2–ZnO showed high photocatalytic activity towards the degradation of C.I. Basic Blue 9, C.I. Basic Red 1, and C.I. Basic Violet 10 dyes [83]. TiO_2 nanoparticles synthesised via the acid-catalysed sol–gel method were used to prepare coupled TiO_2/SiO_2 mesoporous materials were prepared by deposition of TiO_2

nanoparticles. TiO_2/SiO_2 showed photocatalytic activity towards the photodegradation of rhodamine 6G in aqueous solution using UV radiation [84]. One of the noticed studies focuses on TiO_2 nanocomposite with graphene as photocatalyst, one of the most prominent representatives of carbon nanostructures. Coupling TiO_2 with graphene proved to be beneficial, as the higher efficiency in photocatalysis has been observed compared to that of TiO_2 alone. Graphene sheets are thought to act as an electron acceptor that enables the separation and transfer of photogenerated electrons during TiO_2 excitation, simultaneously reducing recombination of electron–hole pairs [87]. Wang et al. reported one of the first studies where TiO_2 (P25)-graphene nanocomposites were used for photocatalytic degradation of methylene blue. Further research has led to the photodegradation of many organic pollutants by these materials [88].

2. Practical Application

The possibility to activate catalysts with sunlight and recent advances in synthesis methods of the catalyst with desirable band gaps opened the opportunity to design prominent solar collectors where photochemical processes are promoted with the absorption of sunlight. While for solar thermal processes, it is essential to collect as many as possible photons of all wavelengths, for the solar photochemical process, it is crucial to collect only high-energy short-wavelength photons, which are responsible for the initiation of photochemical processes. Usually, for the initiation of solar photochemical processes, UV or near UV sunlight is necessary. However, there are some cases where the sunlight of up to 580 nm can be employed, while 600 nm and higher wavelengths are not usable for these purposes [89]. Initially, photoreactors for photochemical applications were based on line-focus parabolic-trough concentrators. This hardware already existed for solar thermal applications and could be easily modified for photochemical processes. The first European facility for water detoxification based on solar photochemical processes was established in Spain by The Centre for Energy, Environmental and Technological Research. Twelve PTCs were used herein while non-concentrating collectors became popular since the influence of concentration and solar tracking does not reduce their efficiency.

Researchers from the Institute of Science and Technology for Ceramics, Italy, developed a TiO_2-coated fabric to be used as a photocatalyst agent to degrade Rhodamine B (RhB) in water. They implemented the obtained photocatalytic materials in a 6 L capacity semi-pilot plant. They evaluated the degradation of RhB dye, simulating the water pollution. The good results encouraged the scale-up of the 6 L semi-pilot plant up to the 100 L pilot plant built [90].

Biologically pretreated industrial wastewater from the factories of the Volkswagen AG in Wolfsburg (Germany) and Taubate (Brazil) has been treated in laboratory conditions with great success, after which a pilot plant was installed in the Wolfsburg factory in 1998 [91]. Another project, called “SOLARDETOX”, is worth mentioning. The name is an abbreviation for Solar Detoxification Technology for the Treatment of Industrial Non-Biodegradable Persistent Chlorinated Water Contaminants. This project aimed to design and develop a commercial non-concentrating solar detoxification system using neither collecting nor non-collecting collectors but compound parabolic collector technology (CPC), having a concentration ratio equal to 1. CPCs present a particular class of solar collectors produced in the shape of two meeting parabolas. The CPC collector belongs to a non-imaging class of collectors

and is considered one of the types with the highest possible concentration ratio. The SOLARDETOX treatment plant is installed at the Hidrocen factory (Madrid, Spain).

Fendrich et al. [92] presented solar concentration technologies for wastewater remediation. They concluded that though mostly on model systems, recent results open promising perspectives for using concentrated sunlight as the energy source powering advanced oxidation processes, such as photocatalytic degradation by TiO_2. Additionally, they identified the photocatalyst materials capable of efficiently working with sunlight and the transition to real wastewater investigation as the most critical issues to be addressed by research in the field.

References

1. Behnajady, M.A.; Modirshahla, N. Kinetic Modeling on Photooxidative Degradation of C.I. Acid Orange 7 in a Tubular Continuous-Flow Photoreactor. Chemosphere 2006, 62, 1543–1548.
2. Xia, X.H.; Liang, Y.; Wang, Z.; Fan, J.; Luo, Y.S.; Jia, Z.J. Synthesis and Photocatalytic Properties of TiO2 Nanostructures. Mater. Res. Bull. 2008, 43, 2187–2195.
3. Ceballos-Chuc, M.C.; Ramos-Castillo, C.M.; Rodríguez-Pérez, M.; Ruiz-Gómez, M.Á.; Rodríguez-Gattorno, G.; Villanueva-Cab, J. Synergistic Correlation in the Colloidal Properties of TiO2 Nanoparticles and Its Impact on the Photocatalytic Activity. Inorganics 2022, 10, 125.
4. Reghunath, S.; Pinheiro, D.; KR, S.D. A Review of Hierarchical Nanostructures of TiO2: Advances and Applications. Appl. Surf. Sci. Adv. 2021, 3, 100063.
5. Verma, R.; Gangwar, J.; Srivastava, A.K. Multiphase TiO2 Nanostructures: A Review of Efficient Synthesis, Growth Mechanism, Probing Capabilities, and Applications in Bio-Safety and Health. RSC Adv. 2017, 7, 44199–44224.
6. Landmann, M.; Rauls, E.; Schmidt, W.G. The Electronic Structure and Optical Response of Rutile, Anatase and Brookite TiO 2. J. Phys. Condens. Matter 2012, 24, 195503.
7. Siddiqui, H. Modification of Physical and Chemical Properties of Titanium Dioxide (TiO 2) by Ion Implantation for Dye Sensitized Solar Cells. In Ion Beam Techniques and Applications; IntechOpen: London, UK, 2019; ISBN 1789845718.
8. Reyes-Coronado, D.; Rodríguez-Gattorno, G.; Espinosa-Pesqueira, M.E.; Cab, C.; De Coss, R.; Oskam, G. Phase-Pure TiO2 Nanoparticles: Anatase, Brookite and Rutile. Nanotechnology 2008, 19, 145605.
9. Navrotsky, A. Energetics of Nanoparticle Oxides: Interplay between Surface Energy and Polymorphism. Geochem. Trans. 2003, 4, 34.
10. Li, J.-G.; Ishigaki, T.; Sun, X. Anatase, Brookite, and Rutile Nanocrystals via Redox Reactions under Mild Hydrothermal Conditions: Phase-Selective Synthesis and Physicochemical Properties.

J. Phys. Chem. C 2007, 111, 4969–4976.

11. Pottier, A.; Chanéac, C.; Tronc, E.; Mazerolles, L.; Jolivet, J.-P. Synthesis of Brookite TiO2 Nanoparticlesby Thermolysis of TiCl4 in Strongly Acidic Aqueous Media. J. Mater. Chem. 2001, 11, 1116–1121.
12. Kondamareddy, K.K.; Neena, D.; Lu, D.; Peng, T.; Lopez, M.A.M.; Wang, C.; Yu, Z.; Cheng, N.; Fu, D.J.; Zhao, X.-Z. Ultra-Trace (Parts per Million-Ppm) W6+ Dopant Ions Induced Anatase to Rutile Transition (ART) of Phase Pure Anatase TiO2 Nanoparticles for Highly Efficient Visible Light-Active Photocatalytic Degradation of Organic Pollutants. Appl. Surf. Sci. 2018, 456, 676–693.
13. Momma, K.; Izumi, F. VESTA 3 for Three-Dimensional Visualization of Crystal, Volumetric and Morphology Data. J. Appl. Crystallogr. 2011, 44, 1272–1276.
14. Hanaor, D.A.H.; Sorrell, C.C. Review of the Anatase to Rutile Phase Transformation. J. Mater. Sci. 2011, 46, 855–874.
15. Siwińska-Stefańska, K.; Krysztafkiewicz, A.; Ciesielczyk, F.; Paukszta, D.; Sójka-Ledakowicz, J.; Jesionowski, T. Physicochemical and Structural Properties of TiO2 Precipitated in an Emulsion System. Physicochem. Probl. Miner. Process. 2010, 44, 231–244.
16. Patra, S.; Davoisne, C.; Bouyanfif, H.; Foix, D.; Sauvage, F. Phase Stability Frustration on Ultra-Nanosized Anatase TiO2. Sci. Rep. 2015, 5, 10928.
17. Holm, A.; Hamandi, M.; Simonet, F.; Jouguet, B.; Dappozze, F.; Guillard, C. Impact of Rutile and Anatase Phase on the Photocatalytic Decomposition of Lactic Acid. Appl. Catal. B Environ. 2019, 253, 96–104.
18. Bhatkhande, D.S.; Pangarkar, V.G.; Beenackers, A.A.C.M. Photocatalytic Degradation for Environmental Applications–a Review. J. Chem. Technol. Biotechnol. Int. Res. Process. Environ. Clean Technol. 2002, 77, 102–116.
19. Lan, Y.; Lu, Y.; Ren, Z. Mini Review on Photocatalysis of Titanium Dioxide Nanoparticles and Their Solar Applications. Nano Energy 2013, 2, 1031–1045.
20. Lydakis-Simantiris, N.; Riga, D.; Katsivela, E.; Mantzavinos, D.; Xekoukoulotakis, N.P. Disinfection of Spring Water and Secondary Treated Municipal Wastewater by TiO2 Photocatalysis. Desalination 2010, 250, 351–355.
21. Chatzitakis, A.; Berberidou, C.; Paspaltsis, I.; Kyriakou, G.; Sklaviadis, T.; Poulios, I. Photocatalytic Degradation and Drug Activity Reduction of Chloramphenicol. Water Res. 2008, 42, 386–394.
22. Vijayabalan, A.; Selvam, K.; Krishnakumar, B.; Swaminathan, M. Photocatalytic Degradation of Reactive Orange 4 by Surface Fluorinated TiO2 Wackherr under UV-A Light. Sep. Purif. Technol.

2013, 108, 51–56.

23. Selvam, K.; Swaminathan, M. Photocatalytic Synthesis of 2-Methylquinolines with TiO2 Wackherr and Home Prepared TiO2–A Comparative Study. Arab. J. Chem. 2017, 10, S28–S34.
24. Vione, D.; Minero, C.; Maurino, V.; Carlotti, M.E.; Picatonotto, T.; Pelizzetti, E. Degradation of Phenol and Benzoic Acid in the Presence of a TiO2-Based Heterogeneous Photocatalyst. Appl. Catal. B Environ. 2005, 58, 79–88.
25. Li, D.; Song, H.; Meng, X.; Shen, T.; Sun, J.; Han, W.; Wang, X. Effects of Particle Size on the Structure and Photocatalytic Performance by Alkali-Treated TiO2. Nanomaterials 2020, 10, 546.
26. Könenkamp, R. Carrier Transport in Nanoporous TiO 2 Films. Phys. Rev. B 2000, 61, 11057.
27. Zhang, K.; Lin, Y.; Muhammad, Z.; Wu, C.; Yang, S.; He, Q.; Zheng, X.; Chen, S.; Ge, B.; Song, L. Active Facet-Exposed Cu2MoS4 Nanotube as High-Efficiency Photocatalyst. Nano Res. 2017, 10, 3817–3825.
28. Che, M.; Védrine, J.C. Characterization of Solid Materials and Heterogeneous Catalysts: From Structure to Surface Reactivity; John Wiley & Sons: Hoboken, NJ, USA, 2012; ISBN 3527645330.
29. Kowalska, E.; Wei, Z.; Janczarek, M. Band-Gap Engineering of Photocatalysts: Surface Modification versus Doping. In Visible-Light-Active Photocatalysis: Nanostructured Catalyst Design, Mechanisms, and Applications; Wiley: Hoboken, NJ, USA, 2018; pp. 449–484.
30. Armaković, S.; Armaković, S.J. Atomistica. Online–Web Application for Generating Input Files for ORCA Molecular Modelling Package Made with the Anvil Platform. Mol. Simul. 2022, 1–7.
31. Tsyshevsky, R.V.; Pagoria, P.; Kuklja, M.M. Computational Design of Novel Energetic Materials: Dinitro-Bis-Triazolo-Tetrazine. J. Phys. Chem. C 2015, 119, 8512–8521.
32. Perdew, J.P. Density Functional Theory and the Band Gap Problem. Int. J. Quantum Chem. 1985, 28, 497–523.
33. Perdew, J.P.; Yang, W.; Burke, K.; Yang, Z.; Gross, E.K.U.; Scheffler, M.; Scuseria, G.E.; Henderson, T.M.; Zhang, I.Y.; Ruzsinszky, A. Understanding Band Gaps of Solids in Generalized Kohn–Sham Theory. Proc. Natl. Acad. Sci. USA 2017, 114, 2801–2806.
34. Perdew, J.P.; Levy, M. Physical Content of the Exact Kohn-Sham Orbital Energies: Band Gaps and Derivative Discontinuities. Phys. Rev. Lett. 1983, 51, 1884.
35. Mori-Sánchez, P.; Cohen, A.J.; Yang, W. Localization and Delocalization Errors in Density Functional Theory and Implications for Band-Gap Prediction. Phys. Rev. Lett. 2008, 100, 146401.
36. Heyd, J.; Scuseria, G.E.; Ernzerhof, M. Hybrid Functionals Based on a Screened Coulomb Potential. J. Chem. Phys. 2003, 118, 8207–8215.

37. Borlido, P.; Aull, T.; Huran, A.W.; Tran, F.; Marques, M.A.L.; Botti, S. Large-Scale Benchmark of Exchange–Correlation Functionals for the Determination of Electronic Band Gaps of Solids. J. Chem. Theory Comput. 2019, 15, 5069–5079.
38. Borlido, P.; Schmidt, J.; Huran, A.W.; Tran, F.; Marques, M.A.L.; Botti, S. Exchange-Correlation Functionals for Band Gaps of Solids: Benchmark, Reparametrization and Machine Learning. npj Comput. Mater. 2020, 6, 96.
39. Cococcioni, M. The LDA+ U Approach: A Simple Hubbard Correction for Correlated Ground States. Correl. Electrons From Model. Mater. Model. Simul. 2012, 2, 1–33.
40. Zhang, R.; Zhao, J.; Yang, Y.; Lu, Z.; Shi, W. Understanding Electronic and Optical Properties of La and Mn Co-Doped Anatase TiO2. Comput. Condens. Matter 2016, 6, 5–17.
41. Chen, W.; Yuan, P.; Zhang, S.; Sun, Q.; Liang, E.; Jia, Y. Electronic Properties of Anatase TiO2 Doped by Lanthanides: A DFT+ U Study. Phys. B Condens. Matter 2012, 407, 1038–1043.
42. Li, Z.; Li, Z.; Zuo, C.; Fang, X. Application of Nanostructured TiO2 in UV Photodetectors: A Review. Adv. Mater. 2022, 34, 2109083.
43. Yang, H.G.; Sun, C.H.; Qiao, S.Z.; Zou, J.; Liu, G.; Smith, S.C.; Cheng, H.M.; Lu, G.Q. Anatase TiO2 Single Crystals with a Large Percentage of Reactive Facets. Nature 2008, 453, 638–641.
44. Zhao, H.; Pan, F.; Li, Y. A Review on the Effects of TiO2 Surface Point Defects on CO2 Photoreduction with H2O. J. Mater. 2017, 3, 17–32.
45. Wrana, D.; Gensch, T.; Jany, B.R.; Cieślik, K.; Rodenbücher, C.; Cempura, G.; Kruk, A.; Krok, F. Photoluminescence Imaging of Defects in TiO2: The Influence of Grain Boundaries and Doping on Charge Carrier Dynamics. Appl. Surf. Sci. 2021, 569, 150909.
46. Wen, B.; Hao, Q.; Yin, W.-J.; Zhang, L.; Wang, Z.; Wang, T.; Zhou, C.; Selloni, A.; Yang, X.; Liu, L.-M. Electronic Structure and Photoabsorption of Ti 3+ Ions in Reduced Anatase and Rutile TiO 2. Phys. Chem. Chem. Phys. 2018, 20, 17658–17665.
47. Dharmale, N.; Chaudhury, S.; Kar, J.K. Various Exchange-Correlation Effects on Structural, Electronic, and Optical Properties of Brookite TiO2. ECS J. Solid State Sci. Technol. 2021, 10, 83010.
48. Armaković, S.J.; Mary, Y.S.; Mary, Y.S.; Pelemiš, S.; Armaković, S. Optoelectronic Properties of the Newly Designed 1, 3, 5-Triazine Derivatives with Isatin, Chalcone and Acridone Moieties. Comput. Theor. Chem. 2021, 1197, 113160.
49. Del Angel, R.; Durán-Álvarez, J.C.; Zanella, R. TiO2-Low Band Gap Semiconductor Heterostructures for Water Treatment Using Sunlight-Driven Photocatalysis. In Titanium Dioxide: Material for a Sustainable Environment; IntechOpen: London, UK, 2018; Volume 305.

50. Etacheri, V.; Di Valentin, C.; Schneider, J.; Bahnemann, D.; Pillai, S.C. Visible-Light Activation of TiO2 Photocatalysts: Advances in Theory and Experiments. J. Photochem. Photobiol. C Photochem. Rev. 2015, 25, 1–29.
51. Yang, H.; Yang, B.; Chen, W.; Yang, J. Preparation and Photocatalytic Activities of TiO2 -Based Composite Catalysts. Catalysts 2022, 12, 1263.
52. Pawar, M.; Topcu Sendoğdular, S.; Gouma, P. A Brief Overview of TiO2 Photocatalyst for Organic Dye Remediation: Case Study of Reaction Mechanisms Involved in Ce-TiO2 Photocatalysts System. J. Nanomater. 2018, 2018, 5953609.
53. Zhang, Z.; Yates, J.T., Jr. Direct Observation of Surface-Mediated Electron− Hole Pair Recombination in TiO2 (110). J. Phys. Chem. C 2010, 114, 3098–3101.
54. Kubovics, M.; Silva, G.; Ana, M.L.; Faria, J.L. Photocatalytic Hydrogen Production Using Porous 3D Graphene-Based Aerogels Supporting Pt/TiO2 Nanoparticles. Gels 2022, 8, 719.
55. Mosquera-Vargas, E.; Herrera-Molina, D.; Diosa, J.E. Structural and Optical Properties of TiO2 Nanoparticles and Their Photocatalytic Behavior under Visible Light. Ing. Compet. 2021, 23, 2.
56. Luttrell, T.; Halpegamage, S.; Tao, J.; Kramer, A.; Sutter, E.; Batzill, M. Why Is Anatase a Better Photocatalyst than Rutile?-Model Studies on Epitaxial TiO2 Films. Sci. Rep. 2014, 4, 4043.
57. Glassford, K.M.; Chelikowsky, J.R. Optical Properties of Titanium Dioxide in the Rutile Structure. Phys. Rev. B 1992, 45, 3874.
58. Bahadoran, A.; De Lile, J.R.; Masudy-Panah, S.; Sadeghi, B.; Li, J.; Sabzalian, M.H.; Ramakrishna, S.; Liu, Q.; Cavaliere, P.; Gopinathan, A. Photocatalytic Materials Obtained from E-Waste Recycling: Review, Techniques, Critique, and Update. J. Manuf. Mater. Process. 2022, 6, 69.
59. Govindasamy, G.; Murugasen, P.; Sagadevan, S. Investigations on the Synthesis, Optical and Electrical Properties of TiO2 Thin Films by Chemical Bath Deposition (CBD) Method. Mater. Res. 2016, 19, 413–419.
60. Soussi, A.; Ait Hssi, A.; Boujnah, M.; Boulkadat, L.; Abouabassi, K.; Asbayou, A.; Elfanaoui, A.; Markazi, R.; Ihlal, A.; Bouabid, K. Electronic and Optical Properties of TiO2 Thin Films: Combined Experimental and Theoretical Study. J. Electron. Mater. 2021, 50, 4497–4510.
61. Huang, F.; Yan, A.; Zhao, H. Influences of Doping on Photocatalytic Properties of TiO2 Photocatalyst. In Semiconductor Photocatalysis-Materials, Mechanisms and Applications; InTech: Rang-Du-Fliers, France, 2016; pp. 31–80.
62. Madima, N.; Kefeni, K.K.; Mishra, S.B.; Mishra, A.K.; Kuvarega, A.T. Fabrication of Magnetic Recoverable Fe3O4/TiO2 Heterostructure for Photocatalytic Degradation of Rhodamine B Dye. Inorg. Chem. Commun. 2022, 145, 109966.

63. Amin, S.; Sher, M.; Ali, A.; Rehman, M.F.; Hayat, A.; Ikram, M.; Abbas, A.; Amin, H.M.A. Sulfonamide-Functionalized Silver Nanoparticles as an Analytical Nanoprobe for Selective Ni (II) Sensing with Synergistic Antimicrobial Activity. Environ. Nanotechnol. Monit. Manag. 2022, 18, 100735.
64. Kumar, A.; Khan, M.; He, J.; Lo, I.M.C. Recent Developments and Challenges in Practical Application of Visible–Light–Driven TiO2–Based Heterojunctions for PPCP Degradation: A Critical Review. Water Res. 2020, 170, 115356.
65. Hua, X.; Liu, Z.; Bruce, P.G.; Grey, C.P. The Morphology of TiO2 (B) Nanoparticles. J. Am. Chem. Soc. 2015, 137, 13612–13623.
66. Goulart, S.; Nieves, L.J.J.; Dal Bó, A.G.; Bernardin, A.M. Sensitization of TiO2 Nanoparticles with Natural Dyes Extracts for Photocatalytic Activity under Visible Light. Dye. Pigment. 2020, 182, 108654.
67. Varshney, G.; Kanel, S.R.; Kempisty, D.M.; Varshney, V.; Agrawal, A.; Sahle-Demessie, E.; Varma, R.S.; Nadagouda, M.N. Nanoscale TiO2 Films and Their Application in Remediation of Organic Pollutants. Coord. Chem. Rev. 2016, 306, 43–64.
68. Žener, B.; Matoh, L.; Reli, M.; Škapin, A.S.; Korošec, R.C. Metal and Non-Metal Modified Titania: The Effect of Phase Composition and Surface Area on Photocatalytic Activity. Acta Chim. Slov. 2022, 69, 217–226.
69. Wu, J.; Lu, S.; Ge, D.; Zhang, L.; Chen, W.; Gu, H. Photocatalytic Properties of Pd/TiO2 Nanosheets for Hydrogen Evolution from Water Splitting. RSC Adv. 2016, 6, 67502–67508.
70. Yu, F.; Wang, C.; Ma, H.; Song, M.; Li, D.; Li, Y.; Li, S.; Zhang, X.; Liu, Y. Revisiting Pt/TiO2 Photocatalysts for Thermally Assisted Photocatalytic Reduction of CO2. Nanoscale 2020, 12, 7000–7010.
71. Sadrieyeh, S.; Malekfar, R. Photocatalytic Performance of Plasmonic Au/Ag-TiO2 Aerogel Nanocomposites. J. Non. Cryst. Solids 2018, 489, 33–39.
72. Cao, X.; Yang, X.; Li, H.; Huang, W.; Liu, X. Investigation of Ce-TiO2 Photocatalyst and Its Application in Asphalt-Based Specimens for NO Degradation. Constr. Build. Mater. 2017, 148, 824–832.
73. Sood, S.; Umar, A.; Mehta, S.K.; Sinha, A.S.K.; Kansal, S.K. Efficient Photocatalytic Degradation of Brilliant Green Using Sr-Doped TiO2 Nanoparticles. Ceram. Int. 2015, 41, 3533–3540.
74. Rossi, L.; Palacio, M.; Villabrille, P.I.; Rosso, J.A. V-Doped TiO2 Photocatalysts and Their Application to Pollutant Degradation. Environ. Sci. Pollut. Res. 2021, 28, 24112–24123.
75. Zheng, S.K.; Wang, T.M.; Hao, W.C.; Shen, R. Improvement of Photocatalytic Activity of TiO2 Thin Film by Sn Ion Implantation. Vacuum 2002, 65, 155–159.

76. Choudhury, B.; Bayan, S.; Choudhury, A.; Chakraborty, P. Narrowing of Band Gap and Effective Charge Carrier Separation in Oxygen Deficient TiO2 Nanotubes with Improved Visible Light Photocatalytic Activity. J. Colloid Interface Sci. 2016, 465, 1–10.
77. Yalçın, Y.; Kılıç, M.; Cinar, Z. The Role of Non-Metal Doping in TiO2 Photocatalysis. J. Adv. Oxid. Technol. 2010, 13, 281–296.
78. Arora, I.; Chawla, H.; Chandra, A.; Sagadevan, S.; Garg, S. Advances in the Strategies for Enhancing the Photocatalytic Activity of TiO2: Conversion from UV-Light Active to Visible-Light Active Photocatalyst. Inorg. Chem. Commun. 2022, 143, 109700.
79. Angela, S.; Lunardi, V.B.; Kusuma, K.; Soetaredjo, F.E.; Putro, J.N.; Santoso, S.P.; Angkawijaya, A.E.; Lie, J.; Gunarto, C.; Kurniawan, A. Facile synthesis of hierarchical porous 2 for simultaneous adsorption and photocatalytic decomposition of crystal violet. Environ. Nanotechnol. Monit. Manag. 2021, 16, 100598.
80. Janczarek, M.; Kowalska, E. On the Origin of Enhanced Photocatalytic Activity of Copper-Modified Titania in the Oxidative Reaction Systems. Catalysts 2017, 7, 317.
81. Tian, Y.; Yang, H.; Wu, S.; Gong, B.; Xu, C.; Yan, J.; Cen, K.; Bo, Z.; Ostrikov, K. High-performance Water Purification and Desalination by Solar-driven Interfacial Evaporation and Photocatalytic VOC Decomposition Enabled by Hierarchical TiO2-CuO Nanoarchitecture. Int. J. Energy Res. 2022, 46, 1313–1326.
82. Humayun, M.; Raziq, F.; Khan, A.; Luo, W. Modification Strategies of TiO2 for Potential Applications in Photocatalysis: A Critical Review. Green Chem. Lett. Rev. 2018, 11, 86–102.
83. Siwińska-Stefańska, K.; Kubiak, A.; Piasecki, A.; Goscianska, J.; Nowaczyk, G.; Jurga, S.; Jesionowski, T. TiO2-ZnO Binary Oxide Systems: Comprehensive Characterization and Tests of Photocatalytic Activity. Materials 2018, 11, 841.
84. Beyers, E.; Biermans, E.; Ribbens, S.; De Witte, K.; Mertens, M.; Meynen, V.; Bals, S.; Van Tendeloo, G.; Vansant, E.F.; Cool, P. Combined TiO2/SiO2 Mesoporous Photocatalysts with Location and Phase Controllable TiO2 Nanoparticles. Appl. Catal. B Environ. 2009, 88, 515–524.
85. Xiong, L.; Yang, F.; Yan, L.; Yan, N.; Yang, X.; Qiu, M.; Yu, Y. Bifunctional Photocatalysis of TiO2/Cu2O Composite under Visible Light: Ti3+ in Organic Pollutant Degradation and Water Splitting. J. Phys. Chem. Solids 2011, 72, 1104–1109.
86. Bessekhouad, Y.; Robert, D.; Weber, J.-V. Photocatalytic Activity of Cu2O/TiO2, Bi2O3/TiO2 and ZnMn2O4/TiO2 Heterojunctions. Catal. Today 2005, 101, 315–321.
87. Padmanabhan, N.T.; Thomas, N.; Louis, J.; Mathew, D.T.; Ganguly, P.; John, H.; Pillai, S.C. Graphene Coupled TiO2 Photocatalysts for Environmental Applications: A Review. Chemosphere 2021, 271, 129506.

88. Wang, W.-S.; Wang, D.-H.; Qu, W.-G.; Lu, L.-Q.; Xu, A.-W. Large Ultrathin Anatase TiO2 Nanosheets with Exposed Facets on Graphene for Enhanced Visible Light Photocatalytic Activity. J. Phys. Chem. C 2012, 116, 19893–19901.
89. Robert, D.; Malato, S. Solar Photocatalysis: A Clean Process for Water Detoxification. Sci. Total Environ. 2002, 291, 85–97.
90. Faccani, L.; Ortelli, S.; Blosi, M.; Costa, A.L. Ceramized Fabrics and Their Integration in a Semi-Pilot Plant for the Photodegradation of Water Pollutants. Catalysts 2021, 11, 1418.
91. Malato, S.; Maldonado, M.I.; Fernandez-Ibanez, P.; Oller, I.; Polo, I.; Sánchez-Moreno, R. Decontamination and Disinfection of Water by Solar Photocatalysis: The Pilot Plants of the Plataforma Solar de Almeria. Mater. Sci. Semicond. Process. 2016, 42, 15–23.
92. Fendrich, M.A.; Quaranta, A.; Orlandi, M.; Bettonte, M.; Miotello, A. Solar Concentration for Wastewaters Remediation: A Review of Materials and Technologies. Appl. Sci. 2018, 9, 118.